Journal of Pharmacological Biomolecules and Therapeutics

ETERNO PRESS

Research

Structure-Based Virtual Screening and ADMET Evaluation of Inhibitors Targeting the Androgen Receptor for Prostate Cancer Therapy

Avinash Kumar[1,*], Kamaljeet Singh[2]

[1]St. Soldier Institute of Engineering & Technology, Jalandhar-Amritsar Bye Pass, NH-1, Behind NIT, Jalandhar City, Punjab, India

[2]College of Pharmacy, Bela, Ropar, Punjab, India

[*]Ccorresponding author: Avinash Kumar, Avinashbad9779@gmail.com

Abstract

Purpose: Persistent activation of the androgen receptor (AR) remains a major driver of prostate cancer progression, particularly in castration-resistant forms, necessitating the development of novel inhibitors with improved efficacy and pharmacokinetic profiles. This study aimed to identify potential AR inhibitors using a structure-based virtual screening approach. Methods: The AR ligand-binding domain (PDB ID: 1Z95) was employed for molecular docking of a designed library of Prostate Specific (PS) analogues using MVD. Drug-likeness was evaluated based on Lipinski's Rule of Five, and top-ranked compounds were further assessed through *in silico* absorption, distribution, metabolism and toxicity (ADMET) profiling to predict pharmacokinetic and toxicity properties. Results: Several PS analogues demonstrated stronger predicted binding affinities than the reference drug bicalutamide (-131.19 kcal/mol), with PS-073 showing the highest MolDock score (-155.84 kcal/mol). Key interactions with residues such as Met745, Gln738, and Leu704 contributed to enhanced binding profiles. Compounds including PS-049, PS-057, and PS-067 exhibited favorable predicted absorption and distribution characteristics, although some analogues showed potential mutagenicity or hepatotoxicity alerts. Conclusion: The identified PS analogues represent promising scaffolds for androgen receptor inhibition, demonstrating improved binding interactions and acceptable predicted pharmacokinetic profiles compared to bicalutamide. However, further experimental validation and structural optimization are required to confirm their therapeutic potential.

Keywords

Androgen Receptor, Prostate Cancer, Bicalutamide, Molecular Docking, ADMET, Virtual Screening, PS Analogues

Article History

Received: 02 April 2026 Revised: 25 May 2026

Accepted: 25 June 2026 Available Online: 09 July 2026

1. Introduction

Cancer remains a leading global health concern, with approximately 20 million new cases and 9.7 million deaths reported in 2022 [1,2]. The incidence is projected to surpass 28 million cases by 2040, driven by aging populations, urbanization, and changing lifestyles [3,4]. It encompasses over 100 disease types characterized by uncontrolled cell growth and spread, with incidence varying by region, sex, and income level [5,6]. Developed countries report higher detection due to better screening programs, while developing regions face rising cases with limited diagnostic resources [7,8]. Cancer arises from a combination of genetic mutations, environmental exposures, and lifestyle factors [9-13]. Major risk contributors include alcohol intake, poor diet, obesity, physical inactivity, and exposure to carcinogens like asbestos or air pollution [14-16]. Infections such as HPV, hepatitis B/C, and *H. pylori* [17-19], along with inherited mutations in genes like BRCA1/2 and TP53, also elevate cancer risk [20-22]. Common global cancers include breast, lung, prostate, liver, and colorectal, with sex-specific patterns influenced by hormonal and biological factors [23-28].

Prostate cancer is the second most common cancer in men and a major cause of male cancer mortality, with 1.46 million new cases and nearly 396,000 deaths in 2022 [29,30]. While more prevalent in developed countries due to PSA screening, cases are rising in developing nations [31-34]. Risk increases with age, particularly after 65 [35-37], and is further influenced by family history, BRCA mutations, race, obesity, and dietary factors [38,39]. Most cases are adenocarcinomas arising from glandular epithelial cells and may range from indolent to highly aggressive, metastatic forms [40-42]. Central to prostate cancer progression is the AR, which regulates gene expression in response to androgens [43,44]. Androgen deprivation therapy (ADT) is the primary treatment [45-47], but resistance often leads to castration-resistant prostate cancer (CRPC), which continues to grow despite low androgen levels [48-50]. CRPC is driven by AR overexpression, mutations, or intratumoral androgen synthesis [51,52]. Early prostate cancer is often silent, found through PSA tests or rectal exams [53]. Advanced stages show urinary issues, bone pain, and fatigue, needing surgery or systemic therapy [54-58]. Despite treatment advances, resistance and side effects remain major concerns [59]. Recent advances in precision oncology have demonstrated that prostate cancer progression is driven by a complex interplay of genomic alterations and AR signaling abnormalities. Key molecular events including AR amplification, AR splice variants such as AR-V7, PTEN loss, TMPRSS2-ERG gene fusion, and BRCA1/2-associated DNA repair defects contribute significantly to tumor aggressiveness, therapeutic resistance, and disease progression. These biomarkers are increasingly integrated into precision diagnostic and prognostic platforms for patient stratification and treatment selection. Despite the clinical success of ADT and second-generation antiandrogens, persistent reactivation of AR signaling remains the dominant driver of CRPC, highlighting the urgent need for structurally optimized AR inhibitors with improved efficacy and pharmacokinetic properties.

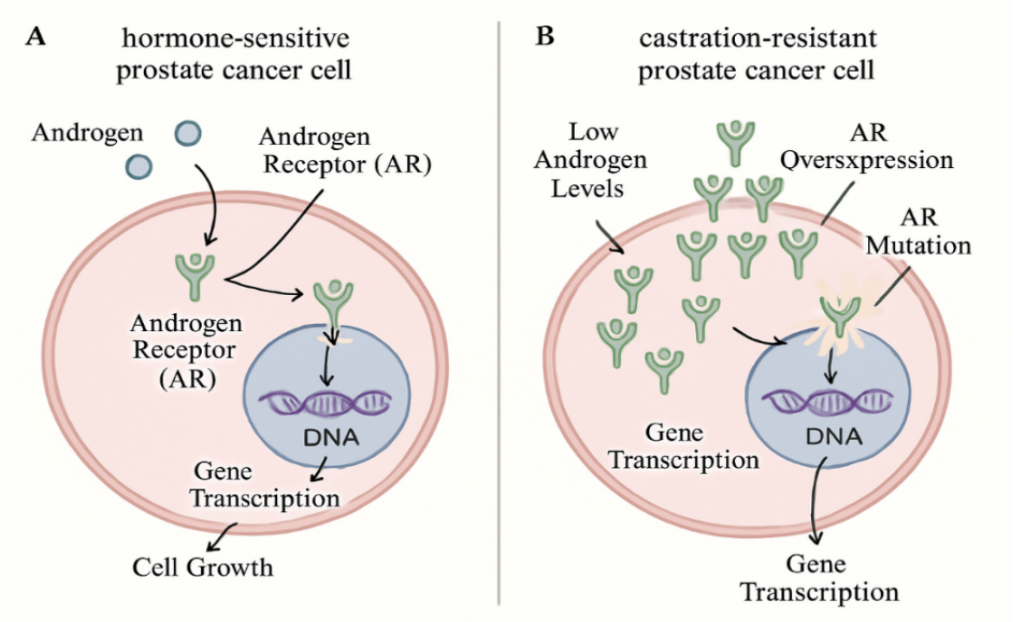

Figure 1. Mechanistic shift from hormone-sensitive to CRPC driven by AR overexpression and mutations enabling persistent transcription despite low androgen levels. (A) Hormone-sensitive prostate cancer cell. (B) Castration-resistant prostate cancer cell.

The evolution from hormone-sensitive to CRPC represents a pivotal shift driven by persistent AR activation despite androgen deprivation. In hormone-sensitive prostate cancer cell (HSPC) (left side), (Figure 1) physiological androgen levels sustain tumour growth through a canonical ligand-dependent mechanism. Circulating testosterone and dihydrotestosterone bind to cytoplasmic AR, inducing conformational changes that promote dissociation from heat shock proteins, receptor dimerization, and nuclear translocation. Inside the nucleus, AR binds to androgen response elements in target gene promoters, recruiting co-activators and transcriptional machinery to drive the expression of genes essential for proliferation, differentiation, and survival. ADT effectively attenuates this signalling by lowering ligand availability. In CRPC (right side), tumour cells circumvent androgen dependence through adaptive molecular

alterations that restore or amplify AR signalling despite castrate serum testosterone levels. Key resistance mechanisms include AR gene amplification leading to receptor overexpression, gain of function mutations that broaden ligand specificity or enable ligand-independent activation, and altered co-regulator recruitment. These adaptations preserve constitutive transcription of oncogenic programs, supporting uncontrolled cell proliferation, metastatic competence, and therapeutic resistance. This persistent AR activity represents a central obstacle to durable disease control and underscores the urgent need for next-generation AR antagonists that can engage the receptor with higher affinity, exploit novel binding epitopes, and retain efficacy against mutant or overexpressed AR forms. While global cancer statistics provide important context, the present study specifically focuses on prostate cancer driven by AR signaling. Therefore, emphasis is placed on molecular mechanisms and therapeutic challenges associated with AR-targeted drug development.

Despite extensive research on AR-targeted therapies, the development of novel scaffolds with improved binding efficiency and pharmacokinetic properties remains a critical challenge. In this context, heterocyclic frameworks such as 1,2,4-oxadiazole have emerged as valuable pharmacophores in medicinal chemistry due to their role as bioisosteres of amide and ester groups. This scaffold contributes to enhanced metabolic stability, optimized lipophilicity, and improved hydrogen bonding capability, which are essential for effective ligand-receptor interactions.

Building on these advantages, the present study focuses on the rational design of PS analogues, incorporating a 1,2,4-oxadiazole core linked through an amide bridge to structurally diverse aromatic systems. This design strategy was aimed at improving interaction complementarity within the AR ligand-binding domain by targeting key residues such as Met745, Gln738, and Leu704. Structural modifications were introduced to balance hydrophobic and electronic properties, thereby enhancing both binding affinity and drug-likeness.

To evaluate these compounds, a structure-based virtual screening approach was employed using the AR ligand-binding domain (PDB ID: 1Z95), followed by molecular docking and *in silico* ADMET profiling. This integrated strategy enables the identification of compounds with improved interaction profiles and acceptable pharmacokinetic characteristics, providing a rational basis for the development of next-generation AR inhibitors.

Computational drug discovery, including structure-based drug design, virtual screening, and *in silico* ADMET analysis, helps identify novel AR inhibitors [60-63]. These tools enable efficient screening of compounds for efficacy and safety. This study applies such methods to discover potential AR-targeting drugs effective against both hormone-sensitive and resistant prostate cancers. The 1,2,4-oxadiazole scaffold proven role as a bioisostere of amide and ester linkages, enhancing metabolic stability, lipophilicity, and facilitating key hydrogen-bond interactions that contribute to broad-spectrum anticancer activity [64].

Unlike previously reported oxadiazole-based antiandrogens, the present PS analogue series was designed with a specific focus on optimizing interaction complementarity within the AR ligand-binding domain through strategic incorporation of amide-linked 1,2,4-oxadiazole cores and diverse aromatic substitutions. This approach emphasizes balancing hydrogen bonding potential and hydrophobic interactions to enhance binding efficiency while maintaining drug-like properties, thereby extending beyond prior designs that primarily focused on substitution effects without integrated structure-based optimization.

Despite extensive research on AR-targeted therapies, significant gaps remain in the development of compounds that combine strong receptor binding with favorable pharmacokinetic and safety profiles. In particular, resistance associated with mutations and altered receptor dynamics continues to limit the effectiveness of existing antiandrogens. This highlights the need for structurally optimized molecules capable of maintaining activity against both wild-type and mutant AR forms.

2. Rationale

In 2024, Kumar S. and Wadhwa P. synthesized a series of 25 novel 3-phenyl-5-styryl-1,2,4-oxadiazole derivatives as non-steroidal anti-androgen agents for prostate cancer treatment. Synthesis involved a three-step process starting from substituted benzonitriles to form amidoximes, followed by reaction with trans-cinnamic acids and cyclization to yield the target oxadiazoles. *In vitro* MTT assays on PC-3 cells showed dose-dependent inhibition, with compound a (fluoro-substituted) being the most potent (IC_{50} = 238.13 nM, 89.99% inhibition), surpassing other compounds but slightly less effective than standard drug bicalutamide (IC_{50} = 158.03 nM, 98.11% inhibition). Compound (a) increased ROS production (55.9% at 300 nM) and reduced AR expression dose-dependently, as confirmed by flow cytometry and immunofluorescence. Molecular docking revealed compound a high binding affinity (-9.5 kcal/mol) to the AR, forming hydrogen bonds with Arg752, Gln711, and Lys808. ADMET analysis indicated favorable drug-like properties for most compounds, with compound (a) adhering to Lipinski's rule and showing high GI absorption and manageable toxicity. The study suggests that fluoro substitution at the *para* position of phenyl ring B enhances activity, likely due to increased electronegativity and favourable interactions with the receptor's active site [65].

In 2024, Khedkar N. R. et al. designed and synthesized a novel series of 3-(4-(4-(1,3,4-oxadiazol-2-yl)-1H-imidazol-2-yl)phenyl)-1,2,4-oxadiazole derivatives for anticancer therapy. The compounds were developed using a fragment-based drug design (FBDD) approach. Synthesis involved a five-step process starting from ethyl 1H-imidazole-4-carboxylate and 4-bromobenzonitrile, using palladium acetate catalysis, hydrazine hydrochloride, and cyclization with aromatic

carboxylic acids. *In vitro* MTT assays on prostate (PC3, DU-145), lung (A549), and liver (HEPG2) cancer cell lines revealed significant cytotoxicity, with many compounds outperforming etoposide. Compound b (3,4,5-trimethoxyphenyl substitution) was the most potent, with IC_{50} values of 0.11 ± 0.039 μM (HEPG2), 0.12 ± 0.095 μM (PC3), 0.13 ± 0.06 μM (A549), and 0.43 ± 0.075 μM (DU-145). All compounds showed high selectivity for cancer cells over normal Vero cells (SI > 9.195-127.27). EGFR inhibitory assays confirmed strong activity against EGFRWT (b: IC50 = 0.102 ± 0.019 μM) but 10-fold lower potency against EGFRT790M (b: IC_{50} = 1.09 ± 0.101 μM). Molecular docking revealed binding affinities comparable to erlotinib (-9.68 kcal/mol), with compound b forming three hydrogen bonds (Met769, Pro770, Lys721) and hydrophobic interactions (Thr830, Leu820, Val702, Val693). Structure-activity relationship (SAR) analysis indicated that electron-donating groups (e.g., 3,4,5-trimethoxy in b) enhanced potency, while electron-withdrawing groups (e.g., 4-chloro, 4-nitro) reduced activity [66].

In 2024, Eeduri R.D. et al. designed and synthesized a series of 10 novel amide derivatives of 1,3,4-oxadiazole-isoxazol-pyridine-benzimidazole *via* a four-step route starting from 1-(1,3,4-oxadiazol-2-yl)ethanone. The synthesis involved Claisen condensation with 5-bromo-1H-benzo[d]imidazole-2-carbaldehyde to form chalcone, cyclization with hydroxylamine hydrochloride to yield isoxazol, Suzuki coupling with pyridin-4-ylboronic acid to produce intermediate, and final amide coupling with substituted benzoyl chlorides to obtain the target derivatives. *In vitro* MTT assays against PC3 (prostate), A549 (lung), MCF-7 (breast), and DU-145 (prostate) cell lines revealed that compound c (3,4,5-trimethoxyphenyl substitution) was the most potent, with IC_{50} values of 0.26 ± 0.08 μM (PC3), 0.11 ± 0.07 μM (A549), 0.87 ± 0.09 μM (MCF-7), and 0.55 ± 0.06 μM (DU-145), outperforming the reference drug etoposide (IC_{50} = 2.39 - 3.08 μM). SAR analysis indicated that EDG, particularly 3,4,5-trimethoxy, enhanced cytotoxicity, while electron-withdrawing substituents decreased activity. Molecular docking showed strong binding of c (binding energies up to -8.87 kcal/mol) with key cancer-related protein residues via hydrophobic interactions, hydrogen bonding, and π-stacking [67].

In 2021, Bommera R.K. et al. designed and synthesized a series of novel 1,2,4-oxadiazole-linked 5-fluorouracil derivatives *via* a three-step route starting from 5-fluorouracil. The synthesis involved alkylation with 4-(bromomethyl)benzonitrile to yield nitrile, conversion to amidoxime with hydroxylamine hydrochloride, and cyclization with substituted benzoic acids in the presence of EDC·HCl and sodium acetate to afford the target derivatives. *In vitro* MTT assays against MCF-7, MDA-MB-231 (breast), A549 (lung), and DU-145 (prostate) cell lines revealed that compound d (3,4,5-trimethoxyphenyl substitution) was the most potent, with IC_{50} values of 0.011 ± 0.009 μM (MCF-7), 0.053 ± 0.0071 μM (A549), 0.017 ± 0.0062 μM (DU-145), and 0.021 ± 0.0028 μM (MDA-MB-231), outperforming etoposide (IC_{50} = 1.91 - 3.08 μM). SAR analysis indicated that EDG, particularly 3,4,5-trimethoxy, markedly enhanced cytotoxicity, whereas EWG reduced activity. Molecular docking with VEGFR-2 showed key hydrogen-bond interactions (Lys866, Gly1046, and Asp1044) and strong binding affinities (Moldock scores up to -157.88 kcal/mol), correlating with biological potency [68].

Current antiandrogens, such as bicalutamide, are limited by their restricted binding interaction diversity, the emergence of drug resistance, and suboptimal pharmacokinetic properties in some patients. To overcome these challenges, a targeted structure-guided design strategy was adopted to develop a novel library of PS analogues. The ligands were rationally constructed through amide bond formation between the COOH group of the acid component and the amine NH_2 group of a 1,2,4-oxadiazole moiety, enabling a stable and conformationally favourable linker that enhances receptor engagement.

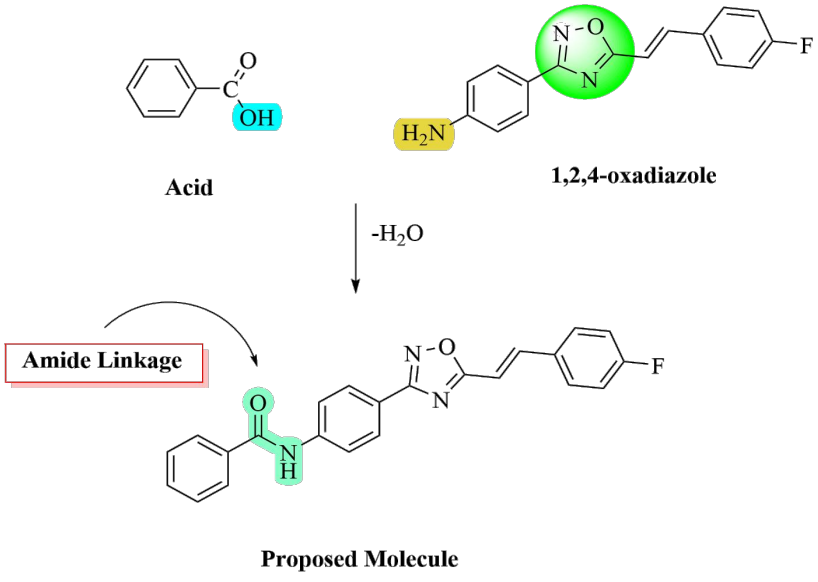

Figure 2. Rational design strategy of PS analogues showing incorporation of a 1,2,4-oxadiazole scaffold linked via an amide bond to diverse aromatic substituents, enabling modulation of electronic properties, hydrogen bonding potential, and hydrophobic interactions within the AR ligand-binding domain.

The oxadiazole fragment was selected for its dual role as a hydrogen bond acceptor/donor and its capacity to modulate lipophilicity and metabolic stability (Figure 2). Using the crystal structure of the AR ligand-binding domain (PDB ID: 1Z95) as a template, substitutions were introduced to improve hydrogen bonding capacity, optimize hydrophobic complementarity, and extend π-π stacking with key residues such as Met745, Gln738, Val903, and Leu704. The design phase was followed by drug-likeness pre-screening via Lipinski's Rule of Five and energy minimization of 3D structures, ensuring favourable physicochemical properties before molecular docking. Integrated computational screening, including docking and *in silico* ADMET profiling, identified lead molecules particularly PS-073, PS-049, PS-067, and PS-057 that exhibited superior binding affinity, broader receptor interaction networks, and improved pharmacokinetic predictions over bicalutamide. This deliberate combination of amide-linked oxadiazole scaffolding and pharmacokinetic optimization enhances translational potential, positioning these PS analogues as promising candidates for further optimization and preclinical evaluation in both hormone-sensitive and resistant prostate cancers. The design of the PS analogues was guided by SAR insights reported for oxadiazole-based antiandrogens, particularly the study by Kumar and Wadhwa (2024), where substitution patterns on aromatic rings significantly influenced biological activity. In that study, electron-donating groups such as fluoro or methoxy substituents enhanced binding affinity and anticancer activity by improving electronic distribution and facilitating favourable interactions within the receptor binding pocket. The SAR analysis demonstrated that fluorine substitution, trimethoxy aromatic groups, and oxadiazole-linked heterocyclic frameworks significantly enhanced anticancer activity through improved hydrophobic interactions, structural stability, and receptor binding affinity (Figure 3A-D).

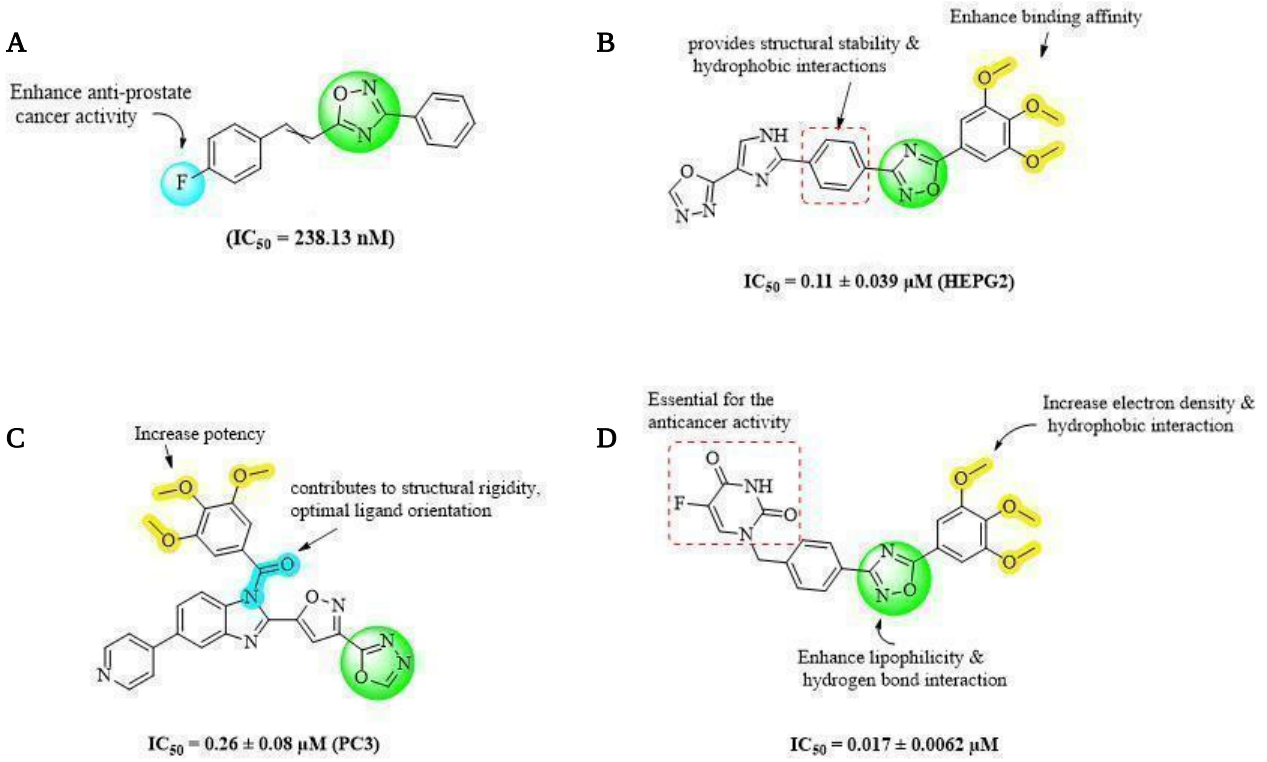

Figure 3. SAR features of representative oxadiazole-based anticancer derivatives: (A) fluorine substitution enhances anti-prostate cancer activity; (B) trimethoxyphenyl substitution improves binding affinity and hydrophobic interactions; (C) oxadiazole-linked heterocyclic framework increases structural rigidity and optimal ligand orientation; and (D) combined trimethoxy and oxadiazole pharmacophores enhance lipophilicity, hydrogen-bonding capability, and overall anticancer potency.

Building on these observations, the present PS analogue series was rationally designed to systematically explore the effect of structural variations on AR binding. Specifically, (i) aromatic substitutions were introduced to modulate hydrophobic interactions with residues such as Val903 and Phe764, (ii) polar functional groups were incorporated to enhance hydrogen bonding with key residues including Met745 and Gln738, and (iii) an amide-linked 1,2,4-oxadiazole core was employed to provide conformational stability while maintaining optimal electronic characteristics.

This integrated design strategy enables correlation of substitution patterns with binding interactions and docking performance, thereby providing a clearer SAR framework compared to earlier studies that primarily focused on isolated substitution effects. Figure 2 illustrates the general design strategy of the PS analogues, highlighting the amide linkage between the carboxylic acid moiety and the 1,2,4-oxadiazole core, along with variable aromatic substitutions introduced to optimize hydrogen bonding and hydrophobic interactions within the AR binding pocket. The present study addresses this gap by applying a structure-based design strategy to develop 1,2,4-oxadiazole-based PS analogues with improved interaction profiles and predicted drug-like properties. This study integrates structure-based virtual screening with *in silico* ADMET analysis to discover novel AR inhibitors for prostate cancer. By targeting the AR ligand-binding site and

analysing efficacy, bioavailability, and safety, the aim is to prioritize compounds with potential against both hormone-sensitive and castration-resistant forms of the disease.

3. Materials and Methods

The AR (Figure 4) was chosen due to its key role in prostate cancer. Its 3D structure (PDB ID: 1Z95, 1.8 Å resolution) was used for precise docking. Protein preparation excluded interfering molecules, and the active site was defined within a 10 Å radius around the native ligand.

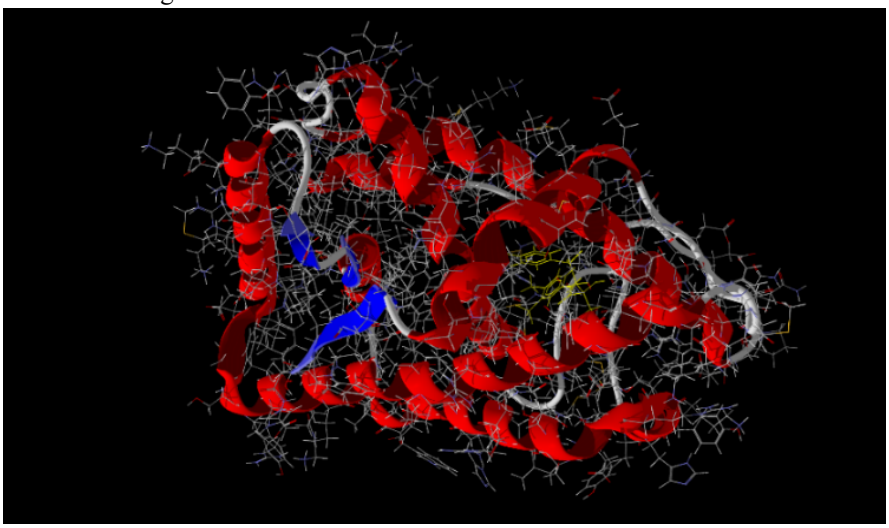

Figure 4. Crystal structure of the AR ligand-binding domain (AR LBD, W741L mutant) in complex with R-bicalutamide (PDB ID: 1Z95), used as the target protein for molecular docking studies.

Molecular docking was performed using Molegro Virtual Docker (MVD), employing a guided differential evolution algorithm for conformational sampling. The AR ligand-binding domain (AR LBD, PDB ID: 1Z95) was prepared by removing the co-crystallized ligand and water molecules, followed by addition of hydrogen atoms and assignment of appropriate charges.

The binding site was defined based on the coordinates of the co-crystallized ligand (R-bicalutamide), ensuring accurate localization of the ligand-binding pocket. A search space with a radius of 10 Å centered on the native ligand position was used to encompass all key interacting residues. Docking simulations were performed with a population size of 50, maximum iterations of 1500, and 10 independent runs per ligand to ensure conformational sampling.

For each compound, multiple binding poses were generated and ranked using the MolDock scoring function. The best pose was selected based on the lowest MolDock score in combination with consistency of key interactions with known binding residues. To improve reliability, rerank scores provided by MVD were also considered during pose evaluation.

A structurally varied ligand library was assembled from literature and chemical databases (Figure S1), prioritizing molecules with potential anti-androgenic or prostate cancer-inhibiting effects. Number of the compounds were curated for drug-likeness based on Lipinski's Rule of Five and similar criteria to improve oral bioavailability, as shown in Table 1. Ligands were manually drawn and converted to 3D structures and then energy minimized with the MM2 method using ChemDraw 3D. Bicalutamide, a clinically established non-steroidal anti-androgen, served as the reference compound. The complete set of designed PS analogues with properly rendered 2D chemical structures is presented in Figure S1 of the main manuscript.

3.1 Process of Docking

Molecular docking was performed using MVD, which employs a guided differential evolution algorithm for conformational searching and scoring. The protocol assumed a flexible ligand and semi-rigid receptor, with a fixed active site and ligand flexibility. Docking parameters included a population size of 50 and up to 1500 iterations per run. Binding affinity of each compound was evaluated using the MolDock scoring function, which estimates binding energy in kcal/mol based on hydrogen bonding. Multiple ligand poses were generated, and the pose with the lowest MolDock score was chosen as the most probable binding conformation (Figure 5).

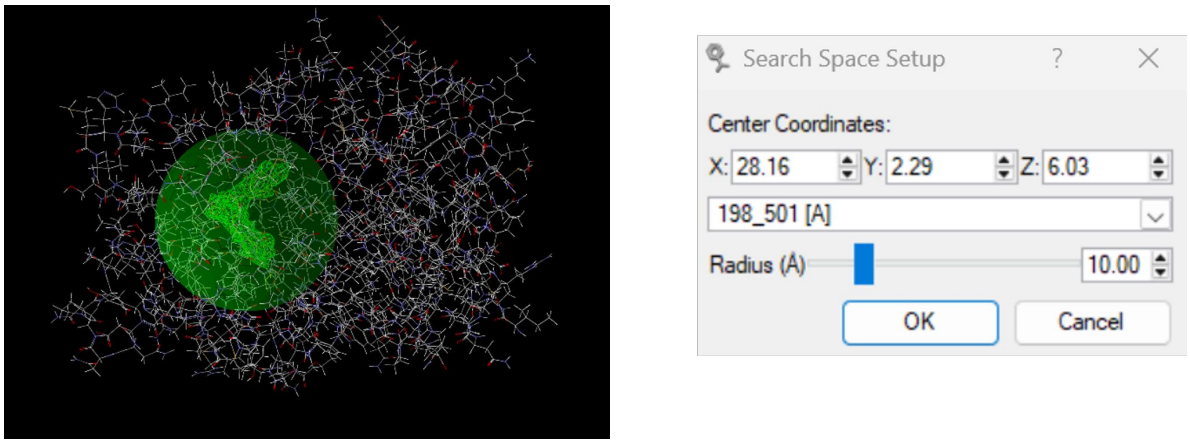

Figure 5. Visualization of the AR ligand-binding cavity showing the docking search space, active site coordinates, and binding region surrounding the co-crystallized ligand in the AR ligand-binding domain (PDB ID: 1Z95).

3.2 Docking Validation

The docking protocol was validated by re-docking the co-crystallized ligand (R-bicalutamide) into the AR ligand-binding pocket after its removal from the crystal structure (PDB ID: 1Z95). The re-docked pose closely reproduced the experimentally observed binding conformation, with a root-mean-square deviation (RMSD) of 1.6 Å, which falls within the accepted threshold (RMSD < 2.0 Å) for reliable docking accuracy (Figure 6).

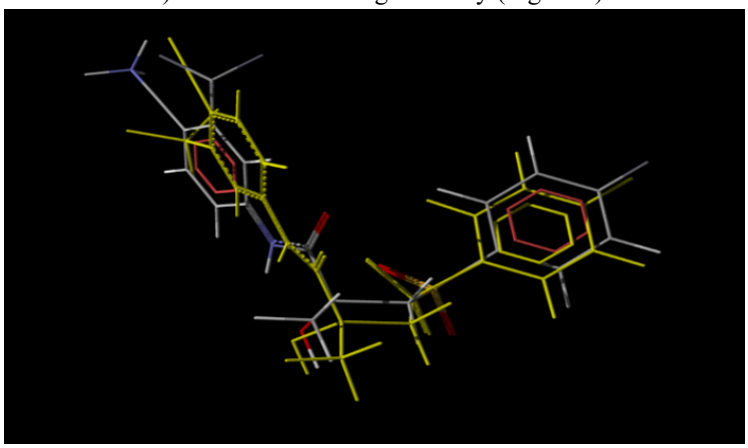

Figure 6. Overlay of the redocked pose (cyan) and the experimentally observed co-crystallized ligand pose (gray) within the AR ligand-binding domain (PDB ID: 1Z95), demonstrating successful validation of the docking protocol.

This agreement confirms that the docking protocol is capable of accurately predicting ligand binding modes within the AR ligand-binding domain. The use of the native ligand to define the binding site further improves the reliability of the docking results by preserving experimentally validated interaction geometry.

4. Results and Discussion

4.1 Molecular Docking Studies

A total of 116 PS analogues were designed and subjected to molecular docking against the AR ligand-binding domain (PDB ID: 1Z95). For clarity, Table 1 presents representative compounds, including the reference drug bicalutamide and selected PS analogues covering high-, medium-, and low-affinity binders. The complete docking dataset for all screened compounds is provided in the Supplementary Information (Table S1).

Bicalutamide, a well-known AR antagonist, serves as the reference compound in due to its favourable pharmacokinetic profile and compliance with Lipinski's Rule of Five shown in Table S1. At the interaction level, bicalutamide forms a hydrogen bond with Asn705 and engages in a steric interaction with Phe764, which together contribute to its receptor antagonism. In contrast, a series of structurally optimized PS series analogues demonstrate both physicochemical variability and enhanced binding interactions. Many of these analogues were specifically designed to interact more extensively with the AR binding pocket, particularly targeting residues such as Gln738, Met745, Val903, and Leu704, which are recurrent across high-affinity ligands. Notably, compounds such as PS-049, PS-067, and PS-089 maintain full compliance with Lipinski's criteria while exhibiting superior molecular interactions compared to bicalutamide. PS-049, with an MW of 418.38 g/mol and a log P of 4.10, forms three hydrogen bonds (Met745, Gln711, Arg752) along with extensive steric contacts with Val903 and Leu704, indicating a stronger and more stable binding profile. Similarly, PS-

067 (MW 445.40 g/mol; log P 4.79) engages in hydrogen bonding with Met745 and forms steric interactions with Gln738, Val903, and Leu704. These enhanced interactions, especially with residues not engaged by bicalutamide, suggest greater potential for receptor inhibition. PS-089 also shows a similar binding pattern with three hydrogen bonds and additional interactions involving His874 and Gln711. These compounds not only outperform bicalutamide in terms of interaction richness but also retain molecular weights below 500 g/mol and log P values within the optimal range, suggesting favourable oral bioavailability. In contrast, analogues such as PS-042 (MW 532.28; log P 7.08) and PS-095 (MW 543.18; log P 6.82) exceed both MW and log P thresholds, violating two Lipinski criteria. Despite forming extensive steric interactions with over ten residues, including Val903, Gln738, and Phe764, these compounds may face limitations in permeability, solubility, and metabolic stability unless supported by formulation strategies. PS-025, although only violating the log P criterion (6.32), forms dual hydrogen bonds with Thr877 and Leu704 and demonstrates strong steric engagement with Val903, Met745, and Gln738, highlighting a potent interaction profile but raising concerns regarding lipophilicity-driven toxicity. On the other hand, compounds such as PS-004 and PS-008, while slightly exceeding the log P threshold (5.92 and 5.45, respectively), compensate through extensive steric interactions with key residues including Tyr739, Val903, and Phe764. PS-008 exhibits interaction with over ten residues, suggesting high binding energy and structural stability within the AR binding pocket. PS-052 and PS-057 also demonstrate dual and triple hydrogen bonding patterns, respectively, while maintaining MW within acceptable range and log P values below 6. PS-057 forms hydrogen bonds with Leu704 and engages sterically with nine residues including Val903, Gln738, and Met745, indicating strong affinity and spatial complementarity with the receptor. Interestingly, while bicalutamide forms only a single hydrogen bond and one steric contact, the majority of PS analogues form interactions with more than six residues, often involving Met745, Leu704, Val746, and Gln738-key residues consistently targeted in high-affinity ligand design. This suggests that the rational design of PS analogues facilitates greater spatial and electrostatic complementarity within the AR binding site, potentially resulting in more robust inhibition. However, not all analogues with enriched binding networks meet drug-likeness criteria. For example, PS-042 and PS-085, despite interacting with ten or more residues, show significant Lipinski violations and may require further optimization or be considered for prodrug development. Conversely, compounds like PS-035, PS-057, and PS-079 demonstrate a balanced profile of improved receptor interactions and acceptable physicochemical properties, with only minor deviations in HBA or HBD and log P values within or slightly above the recommended range. Another notable candidate is PS-073, which forms hydrogen bonds with Gln711 and engages sterically with more than ten residues including Tyr739, Ile906, and His874, while presenting only a single Lipinski violation (log P 5.65), making it a borderline yet promising compound. Collectively, these findings highlight that several PS analogues not only satisfy critical drug-likeness parameters but also establish broader and more potent interaction networks with the AR, potentially leading to improved pharmacodynamic performance. Among them, residues such as Met745 and Gln738 emerge as recurrent anchors, reinforcing their importance in ligand-receptor affinity. The overall comparison clearly indicates that while bicalutamide is an effective AR antagonist with excellent physicochemical properties, it is comparatively limited in interaction diversity. In contrast, PS analogues particularly PS-049, PS-067, PS-089, and PS-057 demonstrate significantly stronger and more diverse receptor interactions while retaining compliance with Lipinski's Rule of Five. The incorporation of additional hydrogen bonding groups and extended aromatic frameworks in these analogues enhances both polar and hydrophobic interactions, expanding their complementarity within the AR binding pocket. These candidates thus represent superior scaffolds for further optimization and development. In conclusion, this direct comparison establishes that selected PS analogues offer significant improvements over bicalutamide in both binding interaction profiles and drug-likeness, providing promising avenues for the development of next-generation antiandrogens for the treatment of prostate cancer (Figure S2).

4.2 *In-silico* ADMET Analysis of the Compounds

ADMET analysis was performed on a subset of compounds selected based on docking performance and drug-likeness criteria. Specifically, compounds with (i) MolDock scores comparable to or better than bicalutamide, (ii) acceptable physicochemical properties (molecular weight < 500 g/mol, log P within a reasonable range), and (iii) favorable interaction profiles with key binding residues were prioritized. This selection approach ensured a balanced evaluation of binding affinity and pharmacokinetic potential. The full ADMET dataset is provided in the (Table 1).

Table 1. Absorption & distribution parameters of selected PS analogs and bicalutamide.

Comp Code	Absorption						Distribution			
	Water solubility	Caco2 permeability	Intestinal absorption (human)	Skin Permeability	P-glycoprotein substrate	P-glycoprotein I inhibitor	VDss (human)	Fu (human)	BBB permeability	CNS permeability
	Numeric (log mol/L)	Numeric (log Papp in 10^{-6} cm/s)	Numeric (% Absorbed)	Numeric (log Kp)	Categorical (Yes/No)	Categorical (Yes/No)	Numeric (log L/kg)	Numeric (Fu)	Numeric (log BB)	Numeric (log PS)
Bicalutamide	-5.50	0.94	82.20	-2.99	Yes	No	-0.78	0.03	-1.26	-2.61
PS-002	-5.97	1.14	92.40	-2.73	Yes	Yes	-0.43	0.04	-0.74	-2.78
PS-004	-6.12	0.47	91.78	-2.73	Yes	Yes	-0.15	0.04	-0.30	-1.56
PS-008	-5.91	1.09	91.59	-2.73	Yes	Yes	-0.49	0.05	-0.70	-2.72
PS-014	-6.19	0.48	92.30	-2.73	Yes	Yes	-0.27	0.03	-0.49	-1.97
PS-016	-5.79	1.06	91.08	-2.73	Yes	Yes	-0.31	0.07	-0.51	-1.70
PS-025	-6.08	0.37	88.95	-2.72	Yes	Yes	-0.19	0.03	-0.69	-1.55
PS-031	-6.12	0.44	90.03	-2.72	Yes	Yes	-0.21	0.04	-0.51	-1.58
PS-035	-4.46	0.05	95.55	-2.74	Yes	Yes	-0.90	0.08	-0.70	-2.10
PS-036	-4.84	0.19	95.71	-2.74	Yes	Yes	-0.51	0.00	-0.55	-1.77
PS-042	-6.19	0.38	87.86	-2.72	Yes	Yes	-0.09	0.03	-0.86	-1.41
PS-044	-5.07	0.50	92.78	-2.74	Yes	Yes	-0.62	0.02	-0.58	-2.81
PS-045	-6.04	0.48	92.27	-2.72	Yes	Yes	-0.27	0.04	-0.49	-1.82
PS-047	-5.94	1.08	91.05	-2.73	Yes	Yes	-0.21	0.05	-0.69	-1.76
PS-048	-4.91	1.16	91.64	-2.73	Yes	Yes	-0.32	0.16	-0.67	-1.87
PS-049	-3.83	0.15	79.28	-2.74	Yes	Yes	-0.55	0.00	-1.64	-3.26
PS-050	-4.93	0.68	91.37	-2.74	Yes	Yes	-0.52	0.02	-0.37	-1.83
PS-051	-5.97	0.37	88.89	-2.72	Yes	Yes	-0.17	0.02	-0.71	-1.64
PS-052	-5.77	0.13	95.11	-2.73	Yes	Yes	-0.51	0.04	-0.93	-2.71
PS-055	-4.08	0.78	98.30	-2.73	Yes	Yes	-0.18	0.05	-1.05	-3.05
PS-057	-5.82	0.51	94.58	-2.74	Yes	Yes	-0.44	0.06	-0.95	-2.95
PS-060	-5.74	0.50	100.0	-2.73	Yes	Yes	-0.29	0.04	-0.45	-1.77
PS-064	-5.99	0.44	91.92	-2.73	Yes	Yes	-0.20	0.05	-0.31	-1.63
PS-067	-4.58	-0.50	93.42	-2.74	Yes	Yes	-0.86	0.00	-0.75	-2.10
PS-073	-6.23	0.44	90.86	-2.73	Yes	Yes	-0.25	0.01	-0.54	-1.95
PS-077	-4.87	0.64	90.83	-2.74	Yes	Yes	-0.60	0.01	-0.38	-1.90
PS-079	-6.08	0.48	91.60	-2.73	Yes	Yes	-0.15	0.05	-0.30	-1.56
PS-085	-6.19	0.37	88.62	-2.72	Yes	Yes	-0.13	0.04	-0.66	-1.45
PS-087	-6.09	0.45	90.09	-2.72	Yes	Yes	-0.23	0.05	-0.51	-1.60
PS-088	-6.22	0.39	90.41	-2.73	Yes	Yes	-0.20	0.04	-0.49	-1.67
PS-089	-3.90	0.16	88.22	-2.74	Yes	Yes	-0.78	0.00	-1.47	-2.85
PS-095	-6.22	0.38	88.85	-2.72	Yes	Yes	-0.10	0.05	-0.66	-1.43
PS-098	-6.08	0.36	89.70	-2.73	Yes	Yes	-0.24	0.04	-0.49	-1.60
PS-100	-6.16	0.41	90.93	-2.72	Yes	Yes	-0.10	0.04	-0.47	-1.50
PS-104	-5.99	0.49	91.92	-2.73	Yes	Yes	-0.20	0.06	-0.32	-1.63
PS-105	-6.04	0.50	91.55	-2.73	Yes	Yes	-0.23	0.05	-0.33	-1.64
PS-110	-4.38	0.39	99.63	-2.74	Yes	Yes	-0.42	0.06	-0.34	-1.86
PS-113	-6.09	0.45	90.09	-2.72	Yes	Yes	-0.23	0.05	-0.51	-1.60
PS-116	-6.12	0.44	90.03	-2.72	Yes	Yes	-0.21	0.04	-0.51	-1.58

4.3 *In Silico* ADMET and Toxicity Prediction

The pharmacokinetic and toxicity profiles of the selected PS analogues were evaluated using the online prediction platform pkCSM and cross-validated with SwissADME for selected physicochemical descriptors and drug-likeness parameters. Canonical SMILES of the designed compounds were generated using ChemDraw and submitted individually for prediction analysis.

Absorption parameters including water solubility, Caco-2 permeability, intestinal absorption, skin permeability, P-glycoprotein substrate/inhibition, and distribution parameters such as volume of distribution at steady state (VDss) and fraction unbound (Fu), blood-brain barrier (BBB) permeability, and CNS permeability were predicted computationally. Metabolism-related endpoints included CYP450 substrate and inhibition profiles, particularly CYP2D6, CYP2C19, and CYP3A4 isoforms. Excretion properties including total clearance and renal OCT2 substrate affinity were also determined.

Toxicity prediction involved assessment of AMES mutagenicity, hERG channel inhibition, hepatotoxicity, skin sensitization, acute oral toxicity (LD_{50}), chronic toxicity (LOAEL), Tetrahymena pyriformis toxicity, and minnow toxicity.

Bicalutamide, a widely used AR antagonist, serves as the reference compound for evaluating the pharmacokinetic performance of the PS analogues. In terms of absorption, bicalutamide shows moderate intestinal absorption (82.2%) and Caco-2 permeability (0.94 log Papp). In comparison, many PS analogues exhibit significantly improved absorption properties. For instance, PS-060 reaches 100% absorption, while compounds such as PS-055 (98.3%), PS-052 (95.11%), and PS-036 (95.71%) demonstrate notably higher absorption rates. Additionally, PS-002 and PS-048 exceed bicalutamide in Caco-2 permeability, with values of 1.14 and 1.16 respectively, indicating superior potential for intestinal epithelial transport and better oral bioavailability. Some analogues like PS-067 and PS-049, despite lower permeability, still maintain acceptable absorption, suggesting alternative transport mechanisms.

Table 2. Metabolic & excretion profiling of select PS analogues and bicalutamide.

Comp Code	Metabolism					Exeretion	
	CYP2D6 substrate	CYP3A4 substrate	CYP2C19 inhibitior	CYP2D6 inhibitior	CYP3A4 inhibitior	Total Clearance	Renal OCT2 substrate
	Categorical (Yes/No)	Categorical (Yes/No)	Categorical (Yes/No)	Categorical (Yes/No)	Categorical (Yes/No)	Numeric (log ml/min/kg)	Categorical (Yes/No)
Bicalutamide	No	No	Yes	No	Yes	0.44	No
PS-002	No	Yes	Yes	No	Yes	0.04	No
PS-004	No	Yes	Yes	No	Yes	0.02	No
PS-008	No	Yes	Yes	No	Yes	-0.20	No
PS-014	No	Yes	Yes	No	Yes	0.11	No
PS-016	No	Yes	Yes	No	Yes	-0.14	No
PS-025	No	Yes	Yes	No	Yes	-0.20	No
PS-031	No	Yes	Yes	No	Yes	-0.56	No
PS-035	No	Yes	Yes	No	Yes	0.04	No
PS-036	No	Yes	Yes	No	Yes	-0.82	No
PS-042	No	Yes	Yes	No	Yes	-0.46	No
PS-044	No	Yes	Yes	No	Yes	-0.03	No
PS-045	No	Yes	Yes	No	Yes	0.04	No
PS-047	No	Yes	Yes	No	Yes	-0.42	No
PS-048	No	Yes	Yes	No	Yes	0.05	No
PS-049	No	Yes	Yes	No	Yes	-0.09	No
PS-050	No	Yes	Yes	No	Yes	-0.04	No
PS-051	No	Yes	Yes	No	Yes	-0.29	No
PS-052	No	Yes	Yes	No	Yes	-0.48	No
PS-055	No	Yes	Yes	No	Yes	0.06	No
PS-057	No	Yes	Yes	No	Yes	0.17	No
PS-060	No	Yes	Yes	No	Yes	0.06	No
PS-064	No	Yes	Yes	No	Yes	0.02	No
PS-067	No	Yes	Yes	No	Yes	-0.04	No
PS-073	No	Yes	Yes	No	Yes	0.15	No
PS-077	No	Yes	Yes	Yes	Yes	-0.05	No
PS-079	No	Yes	Yes	No	Yes	0.02	No
PS-085	No	Yes	Yes	No	Yes	-0.58	No
PS-087	No	Yes	Yes	No	Yes	-0.53	No
PS-088	No	Yes	Yes	No	Yes	-0.46	No
PS-089	No	Yes	Yes	No	Yes	-0.15	No
PS-095	No	Yes	Yes	No	Yes	-0.55	No
PS-098	No	Yes	Yes	No	Yes	-0.27	No
PS-100	No	Yes	Yes	No	Yes	-0.54	No
PS-104	No	Yes	Yes	No	Yes	0.02	No
PS-105	No	Yes	Yes	No	Yes	0.01	No
PS-110	No	Yes	Yes	No	Yes	0.00	No
PS-113	No	Yes	Yes	No	Yes	-0.53	No
PS-116	No	Yes	Yes	No	Yes	-0.56	No

In terms of distribution, the VDss and Fu provide insight into systemic drug availability and tissue penetration. Bicalutamide has a VDss of -0.78 log L/kg and a low unbound fraction of 0.03. In contrast, several PS analogues present higher Fu values, such as PS-048 (0.16), PS-035 (0.08), and PS-036 (0.00), suggesting greater free drug levels

in plasma, which may enhance pharmacological action. VDss values across the PS series are either comparable or more favorable than bicalutamide, indicating improved distribution without excessive tissue accumulation. Furthermore, many analogues show better predicted BBB permeability, a potential advantage in managing metastatic prostate cancer involving the CNS, as shown in Table 2. Overall, the PS analogues exhibit enhanced absorption and distribution characteristics relative to bicalutamide, reinforcing their potential as improved therapeutic candidates in prostate cancer treatment.

Bicalutamide's metabolism and excretion profiles serve as a standard for evaluating the efficiency and safety of newly developed PS analogues. Bicalutamide is not a substrate of major cytochrome P450 enzymes such as CYP2D6 or CYP3A4 but acts as an inhibitor of CYP2C19 and CYP3A4. Its total clearance rate is 0.44 log ml/min/kg, and it is not a substrate of renal OCT2, suggesting hepatic clearance predominance. In contrast, the PS analogues exhibit a consistent metabolic trend. None of the PS compounds are substrates for CYP2D6, aligning with bicalutamide, but all are CYP3A4 substrates. This indicates potential hepatic metabolism via CYP3A4, which may require monitoring for drug-drug interactions if co-administered with CYP3A4 modulators. Like bicalutamide, most PS analogues also inhibit CYP2C19 and CYP3A4, suggesting a comparable inhibitory metabolic pattern.

Table 3. Toxicity predictions for selected PS analogs and bicalutamide including AMES toxicity, maximum tolerated dose, hERG channel inhibition, acute oral toxicity, hepatotoxicity, and aquatic toxicity.

Comp Code	Toxicity									
	AMES toxicity	Max. tolerated dose (human)	hERG I inhibitor	hERG II inhibitor	Oral Rat Acute Toxicity (LD50)	Oral Rat Chronic Toxicity (LOAEL)	Hepatotoxicity	Skin Sensitisation	*T.Pyriformis* toxicity	Minnow toxicity
	Categorical (Yes/No)	Numeric (log mg/kg/day)	Categorical (Yes/No)	Categorical (Yes/No)	Numeric (mol/kg)	Numeric (log mg/kg_bw/day)	Categorical (Yes/No)	Categorical (Yes/No)	Numeric (log ug/L)	Numeric (log mM)
Bicalutamide	No	0.45	No	No	2.85	1.74	Yes	No	0.57	0.08
PS-002	Yes	0.42	No	Yes	2.86	0.77	Yes	No	0.29	-0.94
PS-004	Yes	0.41	No	Yes	2.70	1.00	Yes	No	0.32	-2.12
PS-008	Yes	0.46	No	Yes	2.84	0.76	Yes	No	0.29	-1.04
PS-014	No	0.25	No	Yes	2.71	0.78	Yes	No	0.30	-1.91
PS-016	No	0.45	No	Yes	2.79	0.67	Yes	No	0.30	-1.55
PS-025	Yes	0.40	No	Yes	2.73	0.91	Yes	No	0.31	-1.23
PS-031	Yes	0.42	No	Yes	2.70	0.94	Yes	No	0.31	-1.51
PS-035	Yes	0.28	No	Yes	2.50	3.06	Yes	No	0.29	-1.29
PS-036	Yes	0.17	No	Yes	2.61	2.55	Yes	No	0.29	-2.07
PS-042	Yes	0.35	No	Yes	2.76	0.74	Yes	No	0.31	-1.92
PS-044	Yes	0.32	No	Yes	2.71	2.27	Yes	No	0.29	-0.63
PS-045	Yes	0.41	No	Yes	2.83	0.80	Yes	No	0.30	-0.82
PS-047	No	0.40	No	Yes	2.82	0.48	Yes	No	0.30	-1.62
PS-048	No	0.60	No	Yes	2.80	0.28	Yes	No	0.29	-1.04
PS-049	No	0.28	No	Yes	2.95	3.07	Yes	No	0.29	0.62
PS-050	Yes	0.46	No	Yes	2.71	2.60	Yes	No	0.30	-1.29
PS-051	Yes	0.40	No	Yes	2.65	0.88	Yes	No	0.34	-1.69
PS-052	Yes	0.49	No	Yes	2.85	0.45	Yes	No	0.29	-2.36
PS-055	No	0.46	No	Yes	2.78	0.96	Yes	No	0.30	0.61
PS-057	No	0.37	No	Yes	2.88	0.59	Yes	No	0.29	-0.94
PS-060	Yes	0.33	No	Yes	2.79	1.20	Yes	No	0.32	-1.06
PS-064	Yes	0.42	No	Yes	2.72	1.13	Yes	No	0.32	-1.84
PS-067	Yes	0.04	No	Yes	2.61	3.19	Yes	No	0.29	-1.67
PS-073	No	0.31	No	Yes	2.58	1.11	Yes	No	0.31	-1.43
PS-077	Yes	0.33	No	Yes	2.67	2.71	Yes	No	0.30	-1.56
PS-079	Yes	0.41	No	Yes	2.72	1.07	Yes	No	0.32	-1.94
PS-085	Yes	0.42	No	Yes	2.69	0.79	Yes	No	0.31	-2.52
PS-087	Yes	0.42	No	Yes	2.70	0.97	Yes	No	0.31	-1.36
PS-088	Yes	0.40	No	Yes	2.90	1.01	Yes	No	0.29	-1.84
PS-089	Yes	0.33	No	Yes	2.55	3.03	Yes	No	0.29	-1.01
PS-095	Yes	0.36	No	Yes	2.73	0.81	Yes	No	0.31	-2.79
PS-098	Yes	0.47	No	Yes	2.65	0.96	Yes	No	0.31	-1.83
PS-100	Yes	0.40	No	Yes	2.75	0.93	Yes	No	0.32	-1.94
PS-104	Yes	0.41	No	Yes	2.72	1.12	Yes	No	0.32	-1.84
PS-105	Yes	0.42	No	Yes	2.72	1.09	Yes	No	0.32	-1.15
PS-110	Yes	0.47	No	Yes	2.61	2.79	Yes	No	0.29	-1.60
PS-113	Yes	0.42	No	Yes	2.70	0.97	Yes	No	0.31	-1.36
PS-116	Yes	0.42	No	Yes	2.70	0.94	Yes	No	0.31	-1.51

The excretion profile, particularly total clearance, varies across the PS series. While bicalutamide shows a relatively high clearance (0.44), the PS compounds display a broad range from positive to negative clearance values. For instance, PS-008 and PS-025 show low or negative clearance values (-0.2), suggesting slower elimination, potentially increasing systemic exposure and duration of action. On the other hand, compounds like PS-057 (0.17), PS-073 (0.15), and PS-014 (0.11) demonstrate moderate clearance values closer to bicalutamide, indicating more balanced pharmacokinetics.

Importantly, none of the PS compounds are renal OCT2 substrates, mirroring bicalutamide's profile and indicating limited renal excretion. This Favors hepatic metabolism and may reduce renal burden, which is beneficial in patients with compromised kidney function (Table 3).

The *in-silico* toxicity assessment indicates a mixed safety profile for the PS analogues. While none of the compounds were predicted to inhibit hERG I channels, all analogues showed positive predictions for hERG II inhibition, which may indicate a potential risk of cardiotoxicity that warrants further investigation. Therefore, the absence of hERG I inhibition alone should not be interpreted as confirmation of cardiac safety.

In addition, several compounds exhibited AMES positivity, suggesting potential mutagenicity. Although these predictions are based on computational models and may not directly translate to in vivo outcomes, they represent important structural alerts that should be addressed during lead optimization. Hepatotoxicity was also predicted for multiple compounds, similar to the reference drug bicalutamide, indicating that liver safety remains a relevant consideration for this class of molecules.

Despite these concerns, some compounds such as PS-049, PS-057, and PS-073 demonstrated a relatively balanced toxicity profile when considering all parameters collectively. However, these findings should be interpreted cautiously, as *in silico* toxicity predictions provide preliminary guidance and require experimental validation. Future optimization should focus on reducing mutagenicity risk and minimizing potential cardiotoxic and hepatotoxic liabilities while maintaining binding affinity.

The overall pharmacokinetic and toxicity profiles of the top-performing compounds are summarized graphically in Figure 7, providing a comparative overview of ADMET properties across the selected PS analogues.

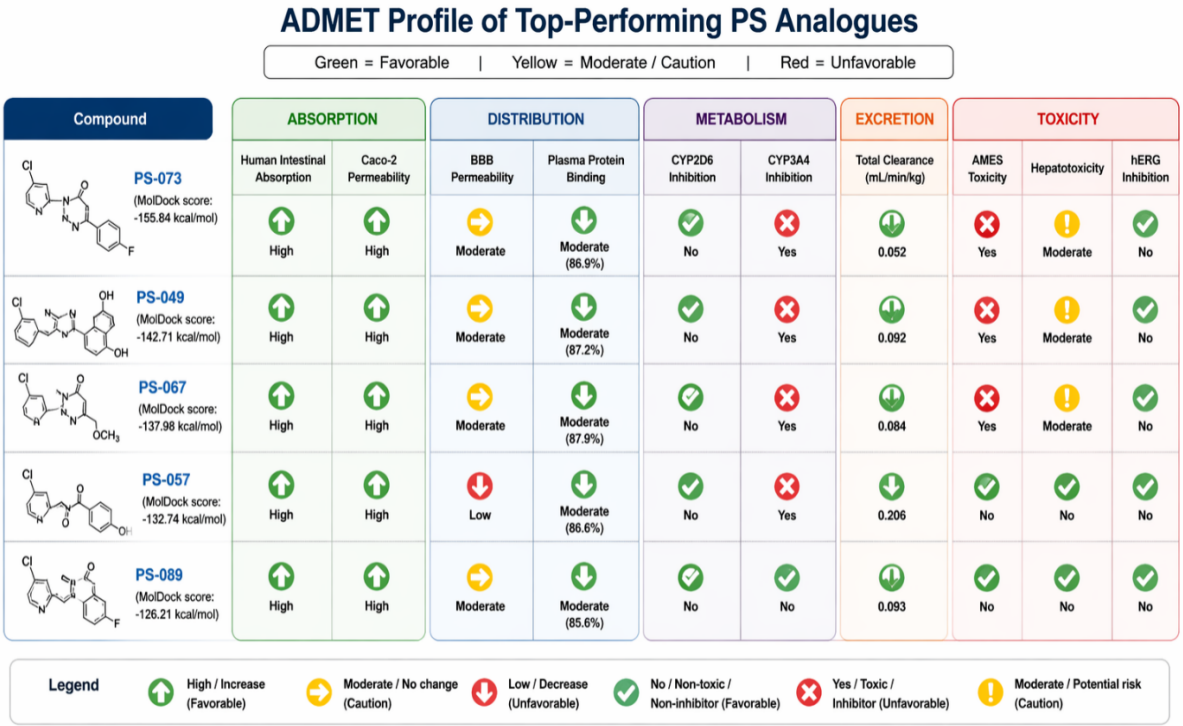

Figure 7. Graphical summary of predicted ADMET (Absorption, Distribution, Metabolism, Excretion, and Toxicity) profiles of top-performing PS analogues (PS-073, PS-049, PS-067, PS-057, and PS-089).

4.4 SAR Interpretation

The SAR analysis reveals that binding affinity is strongly influenced by a balance between hydrophobic interactions and hydrogen bonding capacity. Compounds incorporating extended aromatic systems and hydrophobic substituents, such as PS-073, exhibit enhanced binding due to improved van der Waals interactions within the AR binding pocket, particularly with residues like Val903 and Leu704.

In contrast, the introduction of polar functional groups, as observed in PS-049 and PS-089, increases hydrogen bonding interactions with key residues such as Met745, Gln711, and Arg752, leading to improved binding stability. However,

excessive lipophilicity, as seen in PS-042 and PS-025, while contributing to strong docking scores, may negatively impact drug-likeness and pharmacokinetic behavior.

Overall, compounds demonstrating a balanced physicochemical profile (log P between ~4-5.5) along with multiple interaction types (hydrogen bonding and hydrophobic contacts) show the most favourable combination of binding affinity and drug-like properties. These findings support the importance of optimizing both electronic and steric features to achieve effective AR inhibition. The relationship between structural features and binding performance of the selected compounds is summarized in Table 4, highlighting key determinants influencing AR interaction and docking affinity.

Table 4. SAR analysis of selected PS analogues and reference drug bicalutamide.

Compound	Key Structural Feature	Physicochemical Profile (log P/MW)	Key Interactions (Residues)	H-Bonds	MolDock Score (kcal/mol)	SAR Interpretation
Bicalutamide	Standard non-steroidal scaffold	2.88 / 430.37	Asn705, Phe764	1	-131.19	Limited interaction network
PS-073	Extended aromatic + hydrophobic substitution	5.65 / 441.45	Gln711, Val903, Tyr739, Ile906	1	-155.84	Bulky hydrophobic groups enhance pocket occupancy and binding strength
PS-049	Polar substituents (H-bond donors/acceptors)	4.10 / 418.38	Met745, Gln711, Arg752	3	-142.71	Increased hydrogen bonding significantly improves affinity
PS-067	Balanced aromatic and polar groups	4.79 / 445.40	Met745, Gln738, Val903	1	-137.98	Optimal polarity-lipophilicity balance improves interaction stability
PS-057	Flexible linker with moderate substitution	5.32 / 475.47	Leu704, Val903, Gln738	1	-132.74	Structural flexibility enhances adaptability within binding pocket
PS-089	Polar + aromatic hybrid	4.71 / 417.39	Met745, Gln711, Arg752, His874	3	-126.21	Multiple H-bonds with extended interactions improve binding diversity
PS-042	Highly lipophilic bulky structure	7.08 / 532.28	Val903, Gln711, Met745	0	-145.66	Strong binding but poor drug-likeness due to excessive lipophilicity
PS-025	Dual H-bond donor groups	6.32 / 453.39	Thr877, Leu704	2	-128.37	Increased H-bonding but high log P may limit pharmacokinetics

5. Limitations of the Study

This study is based entirely on computational methodologies, which inherently impose certain limitations. Molecular docking provides an approximate estimation of ligand-receptor binding affinity; however, docking scores alone may not reliably predict true biological activity due to simplified scoring functions, limited treatment of protein flexibility, and neglect of solvent effects. The receptor was treated as largely rigid, which does not fully capture the dynamic nature of protein-ligand interactions.

In addition, molecular dynamics simulations were not performed, and therefore the stability, conformational adaptability, and time-dependent behavior of the ligand-receptor complexes could not be evaluated. This limits confidence in the persistence of predicted binding modes under physiological conditions.

The ADMET properties reported in this study are derived from *in silico* predictive models, which, although useful for early screening, may not accurately reflect in vivo pharmacokinetic and toxicity profiles. Certain predictions, such as mutagenicity and hepatotoxicity, should therefore be interpreted with caution and require experimental validation.

Furthermore, the absence of experimental validation (*in vitro* or *in vivo*) restricts the direct translational applicability of the findings. Consequently, the results of this study should be considered preliminary and hypothesis-generating, serving as a foundation for subsequent experimental and optimization studies.

6. Mechanistic Interpretation of Ligand-Receptor Interactions

A deeper analysis of ligand-receptor interactions reveals that binding affinity of the PS analogues is governed by a combination of hydrogen bonding, hydrophobic interactions, and spatial complementarity within the AR ligand-binding pocket. Among the identified compounds, residues such as Met745, Gln738, Leu704, Val903, and Phe764 consistently emerge as key interaction hotspots, indicating their central role in stabilizing ligand binding.

Compounds exhibiting strong binding affinity, particularly PS-073 and PS-049, demonstrate enhanced interaction networks compared to the reference drug bicalutamide. While bicalutamide forms limited interactions, primarily involving a single hydrogen bond with Asn705, the PS analogues establish multiple contacts, including hydrogen bonds and extensive hydrophobic interactions. For instance, PS-049 forms multiple hydrogen bonds with Met745, Gln711, and Arg752, which likely contribute to increased binding stability through directional interactions. In contrast, PS-073 achieves superior binding affinity primarily through extensive hydrophobic and π-π interactions within the binding cavity, suggesting that optimal pocket filling and van der Waals complementarity play a dominant role in its activity [69,70].

The presence of aromatic moieties in the PS analogues enhances π-π stacking and hydrophobic interactions with residues such as Phe764 and Tyr739, reinforcing ligand anchoring within the binding pocket. Additionally, substitution patterns that balance polarity and lipophilicity appear to be critical. Compounds with moderate lipophilicity (log P ~4-5.5) demonstrate improved interaction profiles, as they maintain sufficient hydrophobic contact without compromising solubility. In contrast, highly lipophilic compounds (e.g., PS-042) exhibit strong docking scores but may suffer from reduced pharmacokinetic suitability.

From a structural perspective, the incorporation of the 1,2,4-oxadiazole scaffold contributes to binding through its ability to act as both a hydrogen bond acceptor and donor, facilitating interactions with polar residues such as Gln738 and Met745. The amide linkage further enhances conformational flexibility, allowing the ligands to adopt favorable orientations within the binding pocket.

These findings suggest that effective AR inhibition is not solely dependent on maximizing docking score but rather on achieving an optimal balance between interaction diversity, structural complementarity, and physicochemical properties. The enhanced interaction profiles observed for selected PS analogues indicate their potential to overcome limitations associated with conventional antiandrogens, particularly those related to limited binding interactions and reduced adaptability within the receptor binding site.

7. Highlights

- Structure-based virtual screening identified novel AR inhibitors from a designed library of PS analogues
- PS-073 exhibited the highest binding affinity (MolDock score: -155.84 kcal/mol), outperforming bicalutamide (-131.19 kcal/mol)
- Key interactions with critical residues such as Met745, Gln738, and Leu704 contributed to enhanced binding profiles
- Several compounds (PS-049, PS-057, PS-067, PS-089) demonstrated a balanced combination of strong binding and favorable drug-likeness
- Predicted ADMET profiles indicated improved intestinal absorption and distribution compared to the reference drug
- Certain analogues showed potential toxicity alerts, highlighting the need for further optimization and experimental validation

8. Conclusion

This study employed a structure-based virtual screening approach to identify potential AR inhibitors based on a series of 1,2,4-oxadiazole-containing PS analogues. Several compounds demonstrated stronger predicted binding interactions within the AR ligand-binding domain compared to the reference drug bicalutamide, with PS-073 showing the most favorable docking score and interaction profile. Key residues such as Met745, Gln738, and Leu704 were consistently involved in ligand binding, highlighting their importance in receptor engagement.

In addition to binding affinity, selected compounds exhibited acceptable predicted pharmacokinetic properties; however, certain analogues showed potential limitations, including Lipinski rule violations, predicted mutagenicity, or hepatotoxicity, indicating the need for further structural optimization. Therefore, the identified compounds should be considered as preliminary leads rather than definitive drug candidates.

Importantly, the findings are based solely on computational methods, and no experimental validation has been performed. Consequently, the observed binding and ADMET profiles require confirmation through in vitro and in vivo studies. While the present work highlights the potential of oxadiazole-based scaffolds for AR targeting, further investigation is necessary to establish their therapeutic relevance, particularly in the context of resistant and mutant AR forms associated with advanced prostate cancer.

Overall, this study provides a rational framework for the identification and optimization of AR inhibitors, offering a foundation for future experimental and medicinal chemistry efforts. It is noteworthy that most PS analogues are predicted to interact with CYP3A4 as substrates and/or inhibitors, which may indicate a potential for drug-drug

interactions. These predictions should be interpreted cautiously, as *in silico* models provide preliminary estimates and require experimental validation. Such interactions may be addressed during lead optimization to minimize metabolic liabilities.

9. Significance of the Study

This study demonstrates the utility of structure-based virtual screening combined with *in silico* ADMET profiling as an efficient strategy for early-stage identification of AR inhibitors. The designed PS analogues, particularly those based on the 1,2,4-oxadiazole scaffold, exhibited enhanced interaction profiles within the AR ligand-binding domain compared to the reference drug bicalutamide, suggesting improved binding complementarity and potential pharmacodynamic advantage.

From a drug discovery perspective, the identification of key interacting residues such as Met745, Gln738, and Leu704 provides actionable insights for rational ligand optimization. The observed balance between hydrogen bonding and hydrophobic interactions in several top-performing compounds highlights critical structural features required for effective AR inhibition [71,72].

Importantly, while some compounds demonstrated favorable predicted pharmacokinetic profiles, the presence of mutagenicity and hepatotoxicity alerts in certain analogues underscores the need for careful optimization. These findings reinforce the importance of integrating both binding affinity and safety considerations during lead selection. Although several compounds exhibited stronger docking scores than bicalutamide, these results represent relative binding estimates within the computational framework and should not be interpreted as direct evidence of superior biological activity.

In a broader context, this work contributes to ongoing efforts to develop next-generation antiandrogen agents capable of addressing limitations associated with current therapies, including resistance in CRPC. Although experimental validation is required, the identified compounds provide a rational starting point for further optimization and preclinical development.

10. Future Perspectives

While the present study identifies promising AR inhibitors through structure-based virtual screening, experimental validation is required to confirm their biological relevance. The top-performing compounds, particularly PS-073, PS-057, PS-049, and PS-067, should be evaluated using in vitro assays in prostate cancer cell lines such as PC-3 and DU-145 to assess cytotoxicity and AR inhibition.

Further investigation through in vivo pharmacokinetic and toxicity studies will be necessary to establish therapeutic potential. In addition, molecular dynamics simulations can provide insight into the stability and conformational behavior of ligand-receptor complexes beyond static docking predictions. Structural optimization strategies should focus on improving solubility, minimizing potential mutagenicity signals observed in some analogues, and enhancing metabolic stability. These steps are essential to advance the identified compounds toward preclinical development.

Funding

Not availed from any source.

Supplementary Materials

Available on request.

Authors Contribution

Kamaljeet Singh: Conceptualization, Methodology, Investigation, Data curation, Writing - Original draft. Avinash Kumar: Formal analysis, Validation, Visualization, Writing - Review & editing.
Thereafter all the authors have agreed to publish this final version of manuscript.

Conflict of Interest

Authors declare no conflict of interest.

Generative AI Statement

Authors have used generative AI model GPT 5 for the language refinement and quality improvement of the manuscript and authors take full responsibility of all the statements included in this manuscript.

Reference

[1] Ibraheem A, Nwosu C, Omowumi R, Ayodapo A. Managing population health through prevention and early detection of cancer and other non-communicable diseases: A call for action. Discover Public Health. 2025, 22(1), 143. DOI: 10.1186/s12982-025-00529-2

[2] Bray F, Laversanne M, Sung H, Ferlay J, Siegel RL, Soerjomataram I, et al. Global cancer statistics 2022: Globocan estimates of incidence and mortality worldwide for 36 cancers in 185 countries. CA: A Cancer Journal for Clinicians. 2024, 74(3), 229-263. DOI: 10.1053/j.gastro.2025.10.014

[3] Sriharikrishnaa S, Suresh PS, Prasada KS, An introduction to fundamentals of cancer biology. Optical Polarimetric Modalities for Biomedical Research. Springer. 2023, 307-330. DOI: 10.1007/978-3-031-31852-8_11

[4] Jain BP, Pandey S. Understanding cancer: From basics to therapeutics. Academic Press. 2022.

[5] Salem HS. Cancer status in the Occupied Palestinian Territories: Types; incidence; mortality; sex, age, and geography distribution; and possible causes. Journal of Cancer Research and Clinical Oncology. 2023, 149(8), 5139-5163. DOI: 10.1007/s00432-022-04430-2

[6] Torre LA, Siegel RL, Ward EM, Jemal A. Global cancer incidence and mortality rates and trends–an update. Cancer Epidemiology, Biomarkers & Prevention. 2016, 25(1), 16-27. DOI:10.1158/1055-9965.EPI-15-0578

[7] Bruni L, Serrano B, Roura E, Alemany L, Cowan M, Herrero R, et al. Cervical cancer screening programmes and age-specific coverage estimates for 202 countries and territories worldwide: A review and synthetic analysis. The Lancet Global Health. 2022, 10(8), e1115-e1127. DOI: 10.1016/S2214-109X(22)00241-8

[8] Shah SC, Kayamba V, Peek Jr RM, Heimburger D. Cancer control in low-and middle-income countries: Is it time to consider screening? Journal of Global Oncology. 2019, 5, 1-8. DOI: 10.1200/JGO.18.00200

[9] Al-Bader SB, Alsulaiman R, Bugrein H, Ben Omran T, Abbaszadeh F, Bakheet N, et al. Cancer genetics program: Follow-up on clinical genetics and genomic medicine in Qatar. Molecular Genetics & Genomic Medicine. 2018, 6, 865-872. DOI: 10.1002/mgg3.534

[10] Tan K, Naylor MJ. The influence of modifiable factors on breast and prostate cancer risk and disease progression. Frontiers in Physiology. 2022, 13, 840826. DOI: 10.3389/fphys.2022.840826

[11] Golubnitschaja O, Kubatka P, Mazurakova A, Samec M, Alajati A, Giordano FA, et al. Systemic effects reflected in specific biomarker patterns are instrumental for the paradigm change in prostate cancer management: A strategic paper. Cancers. 2022, 14(3), 675. DOI: 10.3390/cancers14030675

[12] Valavanidis A. Cancer cases and deaths worldwide attributable to potentially modifiable risk factors. National and Kapodistrian University of Athens. 2024.

[13] Yang X, Man J, Chen H, Zhang T, Yin X, He Q, et al. Temporal trends of the lung cancer mortality attributable to smoking from 1990 to 2017: A global, regional and national analysis. Lung Cancer. 2021, 152, 49-57. DOI: 10.1016/j.lungcan.2020.12.007

[14] Wadgaonkar P. Environmental causes of cancer. Cancer Epigenetics and Nanomedicine. Elsevier. 2024, 69-92. DOI: 10.1016/B978-0-443-13209-4.00017-9

[15] Khokhar A, Sharma P. Role of environmental factors in increased cancer incidences and health impacts. Biotechnological Innovations for Environmental Bioremediation. Springer. 2022, 671-723. DOI: 10.1007/978-981-16-9001-3_28

[16] Du R, Wang Y, Pan M, Zhu J, Zhao Y, Zhang C, et al. Global, regional, and national burdens of pancreatic cancer attributable to smoking from 1990 to 2021 and the projections to 2035: A systematic analysis from the global burden of disease study 2021. Frontiers in Oncology. 2025, 15, 1547029. DOI: 10.3389/fonc.2025.1547029

[17] Hatta MNA, Mohamad Hanif EA, Chin SF, Neoh HM. Pathogens and carcinogenesis: A review. Biology. 2021, 10(6), 533. DOI: 10.3390/biology10060533

[18] Liardo RLE, Borzì AM, Spatola C, Martino B, Privitera G, Basile F, et al. Effects of infections on the pathogenesis of cancer. Indian Journal of Medical Research. 2021, 153(4), 431-445. DOI: 10.4103/ijmr.IJMR_339_19

[19] De Flora S, La Maestra S. Epidemiology of cancers of infectious origin and prevention strategies. Journal of Preventive Medicine and Hygiene. 2015, 56(1), E15-E20.

[20] Freire Chadrina M. Genetic evaluation of young adults with cancer. University of Liege. 2025.

[21] Capoluongo ED, Bazan V. Hereditary cancers. Practical Medical Oncology Textbook. 2021, 65. DOI: 10.1007/978-3-030-56051-5

[22] Gonçalves D, Pires AS, Marques IA, Gomes I, Sousa G, Botelho MF, et al. An overview on radiation sensitivity in hereditary breast and ovarian cancer syndrome. Cancers. 2022, 14(13), 3254. DOI: 10.3390/cancers14133254

[23] Mattiuzzi C, Lippi G. Current cancer epidemiology. Journal of Epidemiology and Global Health. 2019, 9(4), 217-222. DOI: 10.2991/jegh.k.191008.001

[24] Cao W, Chen HD, Yu YW, Li N, Chen WQ. Changing profiles of cancer burden worldwide and in China: A secondary analysis of the global cancer statistics. Chinese Medical Journal. 2021, 134(7), 783-791. DOI: 10.1097/CM9.0000000000001474

[25] Bashar MA, Begam N. Breast cancer surpasses lung cancer as the most commonly diagnosed cancer worldwide. Indian Journal of Cancer. 2022, 59(3), 438-439. DOI: 10.4103/ijc.IJC_83_21

[26] Jackson SS, Marks MA, Katki HA, Cook MB, Hyun N, Freedman ND, et al. Sex disparities in the incidence of 21 cancer types: Quantification of the contribution of risk factors. Cancer. 2022, 128(19), 3531-3540. DOI: 10.1002/cncr.34390

[27] Lopes-Ramos CM, Quackenbush J, DeMeo DL. Genome-wide sex and gender differences in cancer. Frontiers in Oncology. 2020, 10, 597788. DOI: 10.3389/fonc.2020.597788

[28] Kim H-I, Lim H, Moon A. Sex differences in cancer: Epidemiology, genetics and therapy. Biomolecules & Therapeutics. 2018, 26(4), 335. DOI: 10.4062/biomolther.2018.103

[29] Rawla P. Epidemiology of prostate cancer. World Journal of Oncology. 2019, 10(2), 63. DOI: 10.14740/wjon1191

[30] Schafer EJ, Laversanne M, Sung H, Soerjomataram I, Briganti A, Dahut W, et al. Recent patterns and trends in global prostate cancer incidence and mortality: An update. European Urology. 2025, 87(3), 302-313. DOI: 10.1016/j.eururo.2024.11.013
[31] Van Poppel H, Albreht T, Basu P, Hogenhout R, Collen S, Roobol M. Serum PSA-based early detection of prostate cancer in Europe and globally: Past, present and future. Nature Reviews Urology. 2022, 19(9), 562-572. DOI: 10.1038/s41585-022-00638-6
[32] Culp MB, Soerjomataram I, Efstathiou JA, Bray F, Jemal A. Recent global patterns in prostate cancer incidence and mortality rates. European Urology. 2020, 77(1), 38-52. DOI: 10.1016/j.eururo.2019.08.005
[33] Ko L-C, Gravina N, Berghausen J, Abdo J. Rising trends in prostate cancer among Asian men: Global concerns and diagnostic solutions. Cancers. 2025, 17(6), 1013. DOI: 10.3390/cancers17061013
[34] Nyiramana Mukamurera P. Epidemiology of prostate cancer in Africa: An in-depth. Discover the World's Research. 2024, 41(24). DOI: 10.59298/RIJSES/2024/412430
[35] Vickers AJ, Sjoberg DD, Ulmert D, Vertosick E, Roobol MJ, Thompson I, et al. Empirical estimates of prostate cancer overdiagnosis by age and prostate-specific antigen. BMC Medicine. 2014, 12(1), 26. DOI: 10.1186/1741-7015-12-26
[36] DeSantis CE, Miller KD, Dale W, Mohile SG, Cohen HJ, Leach CR, et al. Cancer statistics for adults aged 85 years and older, 2019. CA: A Cancer Journal for Clinicians. 2019, 69(6), 452-467. DOI: 10.3322/caac.21577
[37] Conde-Estévez D, Henríquez I, Muñoz-Rodríguez J, Rodriguez-Vida A. Treatment of non-metastatic castration-resistant prostate cancer: Facing age-related comorbidities and drug–drug interactions. Expert Opinion on Drug Metabolism & Toxicology. 2022, 18(9), 601-613. DOI: 10.1080/17425255.2022.2122812
[38] Sekhoacha M, Riet K, Motloung P, Gumenku L, Adegoke A, Mashele S. Prostate cancer review: Genetics, diagnosis, treatment options, and alternative approaches. Molecules. 2022, 27(17), 5730. DOI: 10.3390/molecules27175730
[39] Al-Ghazawi M, Salameh H, Amo-Afful S, Khasawneh S, Ghanem R. An in-depth look into the epidemiological and etiological aspects of prostate cancer: A literature review. Cureus. 2023, 15(11). DOI: 10.7759/cureus.48252
[40] Humphrey PA. Histopathology of prostate cancer. Cold Spring Harbor Perspectives in Medicine. 2017, 7(10), a030411. DOI: 10.1101/cshperspect.a030411
[41] Surintrspanont J, Zhou M. Prostate pathology: What is new in the 2022 who classification of urinary and male genital tumors? Pathologica. 2023, 115(1), 41. DOI: 10.32074/1591-951X-822
[42] Palmieri C, Fonseca-Alves CE, Laufer-Amorim R. A review on canine and feline prostate pathology. Frontiers in Veterinary Science. 2022, 9, 881232. DOI: 10.3389/fvets.2022.881232
[43] Ehsani M, David FO, Baniahmad A. Androgen receptor-dependent mechanisms mediating drug resistance in prostate cancer. Cancers. 2021, 13(7), 1534. DOI: 10.3390/cancers13071534
[44] Hasan DS. Introduction to cancer biology and genetics: Cancer genetics unlocked. Notion Press. 2024.
[45] Wassersug RJ, Walker LM, Robinson JW, Psych R. Androgen deprivation therapy: An essential guide for prostate cancer patients and their families. Springer. 2023.
[46] Choi E, Buie J, Camacho J, Sharma P, de Riese WT. Evolution of androgen deprivation therapy (ADT) and its new emerging modalities in prostate cancer: An update for practicing urologists, clinicians and medical providers. Research and Reports in Urology. 2022, 87-108. DOI: 10.2147/RRU.S303215
[47] Tortorella E, Giantulli S, Sciarra A, Silvestri I. AR and PI3K/AKT in prostate cancer: A tale of two interconnected pathways. International Journal of Molecular Sciences. 2023, 24(3), 2046. DOI: 10.3390/ijms24032046
[48] Garje R, Riaz IB, Naqvi SAA, Rumble RB, Taplin M-E, Kungel TM, et al. Systemic therapy in patients with metastatic castration-resistant prostate cancer: ASCO guideline update. Journal of Clinical Oncology. 2025, 43(20), 311-2334 DOI: 10.1200/JCO-25-00007
[49] Haque A. Leptin and insulin in advanced prostate cancer: Targeting metabolic response to anti-androgen therapies. Queensland University of Technology. 2025.
[50] Adelian S, Soltani A, Hamblin MR, Chemoresistance, radioresistance, and androgen deprivation therapy resistance in prostate cancer. Prostate Cancer: Molecular Events and Therapeutic Modalities. Springer. 2024, 223-240. DOI: 10.1007/978-981-97-4612-5_11
[51] Khorasanchi A, Hong F, Yang Y, Singer EA, Wang P, Li M, et al. Overcoming drug resistance in castrate-resistant prostate cancer: Current mechanisms and emerging therapeutic approaches. Cancer Drug Resistance. 2025, 8, 9. DOI: 10.20517/cdr.2024.173
[52] Verma S, Prajapati KS, Kushwaha PP, Shuaib M, Singh AK, Kumar S, et al. Resistance to second generation antiandrogens in prostate cancer: Pathways and mechanisms. Cancer Drug Resistance. 2020, 3(4), 742. DOI: 10.20517/cdr.2020.45
[53] Catalona WJ, Richie JP, Ahmann FR, Hudson MLA, Scardino PT, Flanigan RC, et al. Comparison of digital rectal examination and serum prostate specific antigen in the early detection of prostate cancer: Results of a multicenter clinical trial of 6,630 men. The Journal of Urology. 2017, 197(2S), S200-S207. DOI: 10.1016/j.juro.2016.10.073
[54] Gerard S, Mourey L, Briand M, Delaunay B, Balardy L. Prostate diseases. Pathy's Principles and Practice of Geriatric Medicine. 2022.
[55] Huang GJ, Sadetsky N, Penson DF. Health related quality of life for men treated for localized prostate cancer with long-term followup. Journal of Urology. 2010, 183(6), 2206-2212. DOI: 10.1016/j.juro.2010.02.013
[56] Shill DK, Roobol MJ, Ehdaie B, Vickers AJ, Carlsson SV. Active surveillance for prostate cancer. Translational Andrology and Urology. 2021, 10(6), 2809-2819. DOI: 10.21037/tau-20-1370
[57] Klotz L. Active surveillance for prostate cancer: A review. Current urology reports. 2010, 11(3), 165-171. DOI: 10.1007/s11934-010-0110-z
[58] Daly T. Evolution of definitive external beam radiation therapy in the treatment of prostate cancer. World Journal of Urology. 2020, 38(3), 565-591. DOI: 10.1007/s00345-019-02661-6
[59] Oboma YI, Ekpenyong B. Review on gene and cell therapies in prostate cancer treatment: Prospects and challenges. Journal of Translational Genetics and Genomics. 2025, 9(2), 62-75. DOI: 10.20517/jtgg.2024.74
[60] Chunarkar-Patil P, Kaleem M, Mishra R, Ray S, Ahmad A, Verma D, et al. Anticancer drug discovery based on natural products: From computational approaches to clinical studies. Biomedicines. 2024, 12(1), 201. DOI: 10.3390/biomedicines12010201

[61] Zhang W, Lee AM, Jena S, Huang Y, Ho Y, Tietz KT, et al. Computational drug discovery for castration-resistant prostate cancers through in vitro drug response modeling. Proceedings of the National Academy of Sciences. 2023, 120(17), e2218522120. DOI: 10.1073/pnas.2218522120
[62] Shanmuga Sundari M, Thotakura SA, Dharmana M, Gadela P, Ammangatambu MM. Process and applications of structure-based drug design. Artificial Intelligence and Machine Learning in Drug Design and Development. 2024, 321-368. DOI: 10.1002/9781394234196.ch11
[63] Sucharitha P, Reddy KR, Satyanarayana S, Garg T. Absorption, distribution, metabolism, excretion, and toxicity assessment of drugs using computational tools. Computational Approaches for Novel Therapeutic and Diagnostic Designing to Mitigate SARS-CoV-2 infection. Elsevier. 2022, 335-355 .DOI: 10.1016/B978-0-323-91172-6.00012-1
[64] Cherkasova A, Astolfi R, Nawrozkij M, Gladkikh B, Proia E, Giuliani L, et al. 1, 2, 4-oxadiazoles in medicinal chemistry: Trends of the last years. European Journal of Medicinal Chemistry. 2025, 297, 117935. DOI: 10.1016/j.ejmech.2025.117935
[65] Kumar S, Wadhwa P. Synthesis, molecular docking and biological evaluation of 1, 2, 4-oxadiazole based novel non-steroidal derivatives against prostate cancer. Bioorganic Chemistry. 2024, 143, 107029. DOI: 10.1016/j.bioorg.2023.107029
[66] Khedkar NR, Sindkhedkar M, Joseph A. Computational design, synthesis, and assessment of 3-(4-(4-(1, 3, 4-oxadiazol-2-yl)-1 h-imidazol-2-yl) phenyl)-1, 2, 4-oxadiazole derivatives as effective epidermal growth factor receptor inhibitors: A prospective strategy for anticancer therapy. RSC Medicinal Chemistry. 2024, 15(5), 1626-1639. DOI: 10.1039/d4md00055b
[67] Devi ER, Sravani D, Alkhathami AG, Suresh P, Sreenivasulu R, Malladi S, et al. Design, synthesis, *in-vitro* and *in-silico* anticancer studies on amide derivatives of 1, 3, 4-oxadiazole-isoxazol-pyridine-benzimidazole. Chemical Papers. 2025, 79(3), 1385-1405. DOI: 10.1007/s11696-024-03861-0
[68] Bommera RK, Kethireddy S, Govindapur RR, Eppakayala L. Synthesis, biological evaluation and docking studies of 1, 2, 4-oxadiazole linked 5-fluorouracil derivatives as anticancer agents. BMC chemistry. 2021, 15(1), 30. DOI: 10.1186/s13065-021-00757-y
[69] Peng Y, Song Y, Wang H. Systematic elucidation of the aneuploidy landscape and identification of aneuploidy driver genes in prostate cancer. Frontiers in Cell and Developmental Biology. 2022, 9, 723466. DOI: 10.3389/fcell.2021.723466
[70] Abdi N, Alsulami M, Ghaznavi H. Comparing the diagnostic performance of [^{18}F]PSMA-1007 with [^{68}Ga]Ga-PSMA-11 in PET/CT imaging and staging of recurrent prostate cancer. Medicare Advantage. 2025, 3, 9-19. DOI:/10.1002/med4.70006
[71] Peng Y, Dong S, Yang Z, Song Y, Ding J, Hou D. et al. Identification of docetaxel-related biomarkers for prostate cancer. Andrologia. 2021, 53(7), e14079. DOI: 10.1111/and.14079
[72] Zhu J, Liang Z, Song Y, Yang Y, Xu Y, Lu Y, et al. Can the combination of biparametric magnetic resonance imaging and PSA-related indicators predict the prostate biopsy outcome? Andrologia. 2020, 52(10), e13734. DOI: 10.1111/and.13734